PCCP

RSC Publishing

PAPER

Quantification of silanol sites for the most common mesoporous ordered silicas and organosilicas: total *versus* accessible silanols†

Cite this: *Phys. Chem. Chem. Phys.*, 2013, **15**, 642

Matthias Ide,[a] Mohamad El-Roz,[b] Els De Canck,[a] Aurélie Vicente,[b] Tom Planckaert,[a] Thomas Bogaerts,[ae] Isabel Van Driessche,[c] Frédéric Lynen,[d] Veronique Van Speybroeck,[e] Frédéric Thybault-Starzyk[b] and Pascal Van Der Voort*[a]

Received 11th August 2012,
Accepted 7th November 2012

DOI: 10.1039/c2cp42811c

www.rsc.org/pccp

IR and NMR spectroscopy were used to determine the silanol content in the most common mesoporous ordered silicas: MCM-41, MCM-48, SBA-15 and SBA-16. In addition, a spray dried MCM-41 and an ethene bridged PMO are investigated. The results are compared with a commercial chromatographic silica (Nucleosil). The complete distribution of surface and bulk silanols, and of isolated, geminal and vicinal silanols for all these materials is presented. A distinction is made between the *total* silanol number and the *reachable or surface* silanol content. The latter is determined by controlled reactions with simple silanes. All mesoporous ordered silicas, and especially the thick walled SBA-type materials and the PMO contain a surprisingly high amount of total silanol sites, albeit that up to 90% of these silanols are buried inside the walls and are not reachable for small silanes.

1 Introduction

The silanol number is a topic of interest and discussion since the 1950s until today. A good knowledge of the number of silanols on the silica surface is important in areas such as catalysis and adsorption. Also in emerging disciplines, such as drug delivery, tissue engineering by silica and organosilica scaffolds, thin film technology, *etc.*, the exact knowledge of the silanol number is needed or at least desirable. More specifically, in the field of chromatography, the silanol groups are of major importance for two reasons. In the first place, they are the anchoring point for the functional groups of the stationary phase. In this way, they have a direct influence on the retention mechanism of a chromatographic packing material. Secondly, once the functional groups are grafted on the silica surface, it is important that the residual silanol groups are removed from the system by endcapping with *e.g.* a trimethylsilylgroup. This, because residual silanol groups can, for example, lead to asymmetric or tailing signals in the chromatography of basic compounds. On the other hand, in a technique such as capillary electrochromatography (CEC) the remaining silanol groups help to create the electro osmotic flow, which drives the separation.[1]

The determination of the silanol number is complicated by the easy adsorption of water on silica. Therefore the exact quantification with MAS NMR, FTIR, selective chemisorption, deuterium exchange and mass spectroscopy is always complicated by the need for a very controlled atmosphere during sample treatment and measurement. Many models appeared in the 1970s and 1980s on the determination of the silanol number of silica gels or fumed silicas.[2] For silica gels, many different datasets on the silanol number are available, with a large number originating from the former USSR. The silanol number is often referred to as the Zhuravlev number, in honor of his pioneering work in the field.[3] In 1995, Van Der Voort *et al.* published an overview of the silanol number of silica gels as a function of temperature with a specification of the number of isolated, geminal and vicinal silanols.[4] However for the mesoporous ordered (organo)silica materials, prepared by anionic,

[a] *COMOC, Center for Ordered Materials, Organometallics and Catalysis, Department of Inorganic and Physical Chemistry, Ghent University, Krijgslaan 281 (S-3), 9000 Ghent, Belgium. E-mail: pascal.vandervoort@ugent.be; Fax: +32 9264 4983; Tel: +32 9264 4442*

[b] *Laboratoire Catalyse et Spectrochimie (LCS), Université de Caen, 6, Bd du Marechal Juin, 14050 Caen Cedex, France*

[c] *Department of Inorganic and Physical Chemistry, Sol-gel Centre for Research on Inorganic Powder and Thin film Synthesis, University of Ghent, Krijgslaan 281 (S-3), 9000 Ghent, Belgium*

[d] *Department of Organic Chemistry, Laboratory of Separation Sciences, University of Ghent, Krijgslaan 281 (S-4), 9000 Ghent, Belgium*

[e] *Center for Molecular Modeling, Ghent University, Technologiepark 903, 9052 Zwijnaarde, Belgium*

† Electronic supplementary information (ESI) available. See DOI: 10.1039/c2cp42811c

cationic or neutral templates at a wide range of pH values and temperatures, this table is no longer applicable, as we will show in this work.

Several standard methods have been used to characterize and quantify the density of silanol groups of both amorphous and mesostructured silica materials. Thermogravimetric analyses,[5] diffuse reflectance Fourier transform infrared spectroscopy (DRIFT),[6] ^{29}Si and ^{1}H NMR,[7] microcalometry[8] or a combination of these techniques were combined with the use of probing molecules such as silanes,[9] water[10] or pyridine[11] adsorption. The silanol concentrations that have been reported on MCM-41 are hardly comparable, due to the fact that each paper reports a different silanol number for MCM-41 without considering synthesis and analysis parameters.[12] For example the silanol number is strongly dependent on the temperature of any post synthesis treatment.[4] However in six different reports where MCM-41 was post treated at the same temperature, silanol values varying from 0.9 up to 3 groups per nm^2 were found.[5,11,13] After a thorough search of the literature, no systematic determination of the silanol number of periodic mesoporous organosilicas could be found. Also a systematic comparison of the most common mesoporous ordered silicas is not available in the literature.

Therefore in this contribution, we report the *accessible surface silanols* for various chromatographic relevant functional groups together with the *total amount of silanol groups*, whether they are on the surface or not. We believe this information will be useful for many colleagues in various fields of research and for the chromatographic colleagues in particular. The silanol numbers have been quantified using previously described IR techniques[14] combined with solid state NMR and elemental analysis of grafting procedures.

2 Experimental

2.1 Materials

Nucleosil 300-5 (mean pore diameter: 30 nm; 5 μm particle size) was purchased from Macherey-Nagel. Hexadecyltrimethylammonium bromide (99%) (CTAB), tetraethyl orthosilicate (98% reagent grade) (TEOS), ammonium hydroxide, potassium chloride (>99%) acetonitrile (HPLC grade), 1-butanol (99.8%), pluronic $PEO_{20}PPO_{70}PEO_{20}$ (P123), pluronic $PEO_{106}PPO_{70}PEO_{106}$ (F127), vinyltriethoxysilane (VTES) and Grubbs' 1st generation catalyst were acquired at Sigma-Aldrich. Fuming hydrochloric acid 37 w/w% was purchased from Roth, anhydrous toluene (>99.9%) for the grafting was obtained from Acros. *n*-Octadecyldimethylchlorosilane (97%), *n*-octyldimethylchlorosilane and bis(trimethylsilyl) amine were supplied by ABCR. All chemicals were used without further purification.

2.2 Synthesis of the supports

SBA-15,[15] SBA-16,[16] MCM-41,[17] MCM-48,[18] spray dried MCM-41[19] and ethene bridged periodic mesoporous organosilica (PMO)[20] were all prepared according to methods found in the literature. All syntheses were carried out under hydrothermal conditions, except for the spray dried MCM-41 type material, denoted as MCM-41(SD). Three types of pore systems were synthesized, a hexagonal and two cubical pore systems. MCM-41, MCM-41(SD), SBA-15 and the ethene bridged PMO have a hexagonal pore system. The MCM-48 and the SBA-16 both exhibit a cubical pore system. All the synthesis procedures can be found in the ESI.† Nucleosil 300-5 is commonly used as a packing material in chromatographic HPLC applications. MCM-41, MCM-41(SD), MCM-48, SBA-15 and SBA-16 were calcined at 550 °C for 6 hours with a heating rate of 1.5 °C per min to remove the surfactant. The surfactant of the ethene bridged PMO was removed by a soxhlet extraction with acetone.[21] After the synthesis all the samples were kept dry under inert atmosphere (Ar).

2.3 Grafting procedures

Prior to grafting, water was removed from the samples by a heating procedure at 120 °C under vacuum conditions for 24 hours.

Three different silanes with increasing tail length were used as probing molecules to determine the amount of accessible silanol sites on the surface of the different silica materials. A trimethylsilyl (C3), an octyldimethylsilyl (C8) and an octadecyldimethylsilyl (C18) group were anchored to the surface. The reaction time was 24 h for all the grafting reactions and the composition of the final mixture was 0.5 g silica/1.4 mmol silane/30 ml solvent. The trimethylsilyl and the octyldimethylsilyl groups were grafted by means of hexamethyldisilazane and octyldimethylchlorosilane, respectively, in dry acetonitrile and left to stir for 24 hours at room temperature. The octadecyldimethylsilyl group was grafted by means of octadecyldimethylchlorosilane in dry toluene under the same conditions as cited above.

After reaction, the materials were filtered off, washed thoroughly with acetonitrile or toluene and acetone, dried at 120 °C under vacuum and analyzed with elemental analysis.

2.4 Characterization

Nitrogen adsorption experiments were measured at −196 °C using a Belsorp mini II gas analyzer. X-ray powder diffraction (XRPD) patterns were collected on an ARL X′TRA X-ray diffractometer with Cu Kα radiation of 0.15418 nm wavelength and a solid-state detector. Elemental analyses (C, H) were performed on a Thermo Scientific Flash 2000 CHNS-O Analyzer.

For the determination of the silanol number, a special transmission FTIR setup was used. The silica powders were pressed ($\sim 10^7$ Pa) into self-supported discs (2 cm^2 area, 7–8 mg cm^{-2}). They were placed in a cell equipped with KBr windows. A movable quartz sample holder allowed placing the pellet in the infrared beam, for recording spectra, and moving it into a furnace at the top of the cell for thermal treatment (see Fig. 1).

A Nicolet 6700 IR spectrometer equipped with a DTGS detector and an extended-KBr beam splitter was used for the acquisition of spectra recorded in the 400–5500 cm^{-1} range. Spectra were recorded at 4 cm^{-1} and 250 scans were co-added for each spectrum.

Solid-state MAS NMR spectra were recorded on a Bruker Avance-400 (9.4 T) spectrometer using 4 mm-OD zirconia rotors and a spinning frequency of 12 kHz. Single pulse

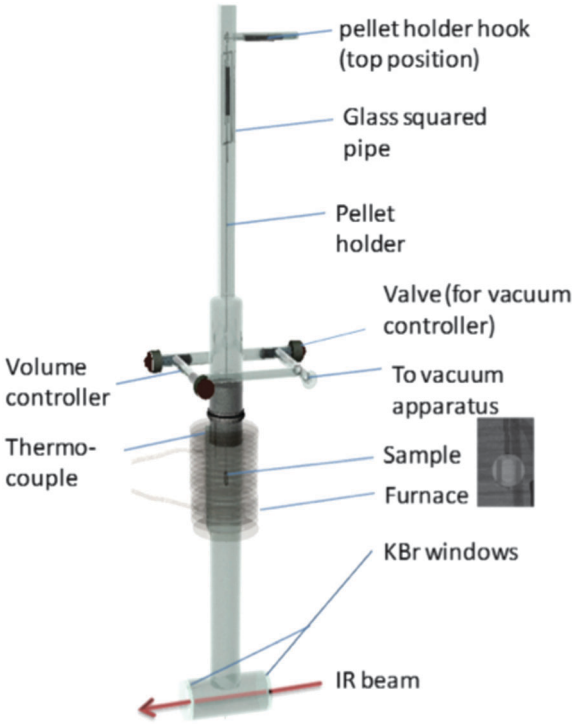

Fig. 1 The *in situ* IR-cell used to determine the silanol number of the materials.

excitation (30° flip angle) and 20 s recycling delay was used for ^{29}Si MAS NMR experiments. {^{1}H}-^{29}Si cross-polarization (CP) MAS experiments were performed using a contact time of 6 ms and a recycle time of 3 s. Tetramethylsilane (TMS) was used as chemical shift reference for the ^{29}Si nuclei.

3 Results and discussion

In order to simplify the discussion of the effect of the synthesis method on the material properties, the main differences between synthesis conditions and template removal are summarized in Table 1.

As mentioned above in the experimental part, the template removal has been performed by conventional calcination at 550 °C, except the PMO which was activated by soxhlet extraction using acetone as solvent. The comparison of the MCM-41 and MCM-41(SD) allows understanding the effect of hydrothermal and spray dried synthesis on the material behavior. For comparison, Nucleosil was purchased from Macherey-Nagel in order to be used as a reference.

Table 1 Overview of the materials: synthesis conditions and template removal

Material	Synthesis conditions		Template removal
SBA-15	Hydrothermal	Acid	Calcination
SBA-16	Hydrothermal	Acid	Calcination
MCM-41	Hydrothermal	Base	Calcination
MCM-48	Hydrothermal	Base	Calcination
MCM-41(SD)	Spray dried	Acid	Calcination
EthenePMO	Hydrothermal	Acid	Extraction

3.1 The pore properties of the materials

Three types of pore structures were synthesized, a hexagonal *P6/mm* structure (MCM-41-HT, MCM-41-SD, SBA-15 and ethene bridged PMO) and two cubical structures (MCM-48 (*Ia3d*) and SBA-16 (*Im3m*)). The materials were all synthesized according to their most common ways of synthesis as found in the literature.

The various pore properties are shown in Table 2, the surface area ($SA_{(BET)}$), pore volume (V_p) and pore diameter (d_p) were determined with N_2-sorption. The unit cell (a_0) was determined from the XRD spectra of the materials and the wall thickness (h) was calculated with the following formulas:

- MCM-41, SBA-15 and ethene bridged PMO:[22] $h = a_0 - 0.95d_p$
- MCM-48:[23] $h = \frac{a_0}{3.0919} - \frac{d_p}{2}$
- SBA-16:[24] $h = \frac{\sqrt{3}}{2}a_0 - d_p$

Note that for Nucleosil no pore diameter could be calculated due to its broad pore size distribution. This material is also unordered, and does not produce any XRD reflections.

3.2 The total concentration of silanol groups from *in situ* IR

According to the literature,[14] adsorbed water species are characterised by a δH_2O band near 1630 cm^{-1} (Fig. 2a). The spectrum of the dried sample (Fig. 2b) presents a narrow band at 3740 cm^{-1} characterizing isolated silanol groups.

The band of inner hydroxyl groups is situated at about 3650 cm^{-1}. The band of H-bonded hydroxyl groups is situated

Table 2 The pore properties of the various materials, with the surface area SA_{BET}, the pore volume V_p, the pore diameter d_p, the unit cell a_0 and the wall thickness h

Material	SA_{BET} (m^2 g^{-1})	V_p (cm^3 g^{-1})	d_p (nm)	a_0 (nm)	h (nm)
SBA-15	656	0.7	6.9	10.7	4.2
SBA-16	738	0.6	6.2	14.6	6.4
MCM-41	1144	0.6	2.9	3.8	1.1
MCM-48	1293	0.8	2.8	7.3	1.0
MCM-41(SD)	719	0.4	2.9	3.6	1.2
EthenePMO	923	1.0	6.2	9.0	3.1
Nucleosil	88	0.4	—	—	—

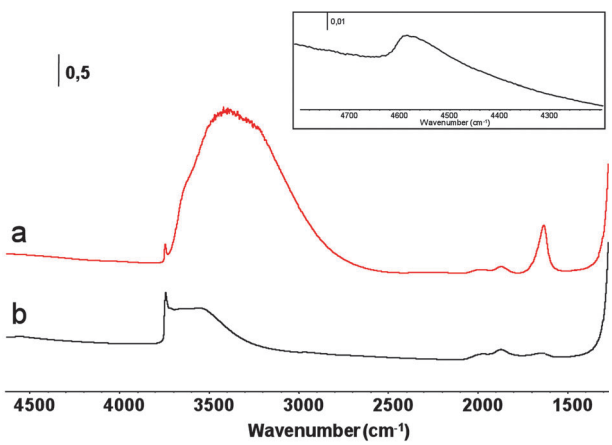

Fig. 2 Infrared spectra of SBA-15 sample in the 1500–4500 cm^{-1} range. (a) Spectrum recorded under atmosphere conditions. (b) Spectrum recorded after degassing at 10^{-5} hPa for 1 h at room temperature.

Table 3 The silanol number and the Q^2, Q^3 and Q^4 species in the material

Material	1 Silanol content (IR) α_{OH} (mmol g^{-1})	2 Q^3/Q^4	3 Q^2/Q^4	4 SiO_3OH (%) $Q^3/(Q^2 + Q^3)$	5 $SiO_2(OH)2$ (%) $Q^2/(Q^2 + Q^3)$	6 Total SiOH ratio $(2Q^2 + Q^3)/(Q^2 + Q^3 + Q^4)$	7 Condensation degree $Q^4/(Q^2 + Q^3 + Q^4)$
SBA-15	3.5	0.30	0.04	88	12	0.28	0.75
SBA-16	8.3	0.52	0.02	96	4	0.37	0.65
MCM-41	3.6	0.82	0.06	94	6	0.49	0.53
MCM-48	5.2	0.67	0.04	94	6	0.44	0.58
MCM-41(SD)	3.2	0.35	0.01	97	3	0.27	0.74

Table 4 The silanol number and the T^1, T^2 and T^3 species in the material

Material	1 Silanol number (IR) α_{OH} (mmol g^{-1})	2 T^2/T^3	3 T^1/T^3	4 SiO_2OH (%) $T^2/(T^1 + T^2)$	5 $SiO_1(OH)_2$ (%) $T^1/(T^1 + T^2)$	6 Total SiOH ratio $(2T^1 + T^2)/(T^1 + T^2 + T^3)$	7 Condensation degree $T^3/(T^1 + T^2 + T^3)$
EthenePMO	16.9	1.16	0.06	95	5	0.66	0.45

at about 3540 cm^{-1}. From the area of the $(\nu + \delta)$ OH band at 4560 cm^{-1} (inset of Fig. 2), we have estimated the total concentration of Si–OH groups (both on the surface and in the wall) (Tables 3 and 4, column 1), using the methodology described in ref. 14. In this way, there is no bias from a possible contribution of physisorbed water.

3.3 The various OH species according to MAS ^{29}Si NMR

The OH species were quantified using MAS ^{29}Si NMR and the NMR band was located using CP MAS $\{^1H\}$-^{29}Si. The CP MAS $\{^1H\}$-^{29}Si is a technique that highlights the presence of OH groups, which elucidates the ^{29}Si MAS spectrum. Just as it is the case with the *in situ* IR measurements, solid state NMR is a bulk analysis tool. It measures both the silanols on the surface and in the walls of the materials. However, only silicon ratios are measured with solid state NMR.

The OH species for MCM and SBA materials. First the pure silica materials (MCM and SBA type) are compared. Spectra obtained by direct polarization and by CP-MAS are presented in Fig. 3A and B, respectively. Fig. 4 depicts the NMR spectra for the silica materials with the Q^2, Q^3 and Q^4 sites, as well as schematic representation of these three species. From the integration of the three different peaks obtained in each sample it has been possible to estimate the relative amount of each species. The quantification results are then presented in Table 3.

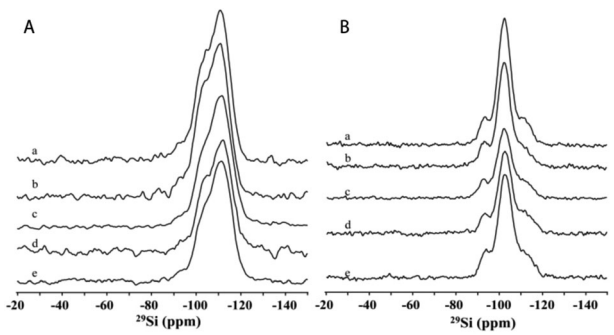

Fig. 3 The ^{29}SiMAS NMR (A) and the CPMAS $\{^1H\}$-^{29}Si (B) spectrum for MCM-41HT (a), MCM-48 (b), MCM-41SD (c), SBA-15 (d) and SBA-16 (e).

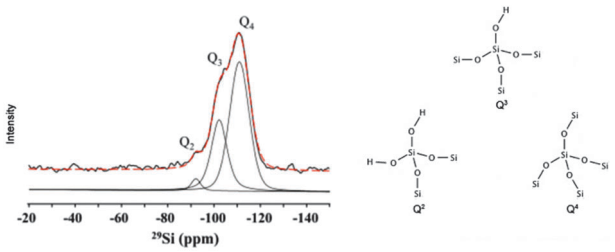

Fig. 4 The allocation of the Q^2, Q^3 and Q^4 site on the NMR spectra of the MCM and SBA materials.

Column 1 shows the silanol concentration acquired with infrared spectroscopy. This is the total silanol content, so both the surface silanols and the ones in the wall. A general trend visible in these data is that thick walled materials (SBA type materials) exhibit a higher number of total silanol groups.

Columns 2 and 3 depict the Q^3 : Q^4 and Q^2 : Q^4 ratios of the various materials. The thin-walled MCM materials exhibit a much higher percentage of surface silicon atoms, due to thinner walls. A rough estimate of the percentage of surface silicon atoms is shown in ESI† (Table S1). They therefore also have a much higher percentage of Q^3-sites than the thick-walled SBA-type materials. Since silanol groups are preferentially at the surface it can be understood that MCM materials exhibit a slightly higher Q^3 : Q^4 ratio than SBA materials. Columns 4 and 5 depict the separate percentages of $SiO_2(OH)_2$ and SiO_3OH species, respectively, indicated as geminal and single silanols. The total SiOH ratio $(2 \times SiO_2(OH)_2 + SiO_3OH)$ is shown in column 6. The last column (7) is designated as the condensation degree. The condensation degree is larger for hydrothermally synthesized SBA materials in comparison with hydrothermal MCM materials. Because the wall thickness of SBA materials is higher than MCM materials this indicates that the total amount of hydroxylated silicon atoms lowers with the wall thickness. Therefore it can be concluded that the main part of the silanol groups is situated at the pore wall/air interface.

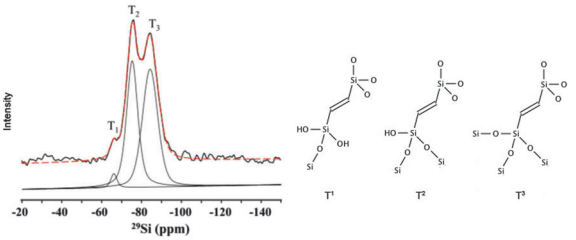

Fig. 5 The allocation of the T^1, T^2 and T^3 site on the NMR spectra of the PMO material.

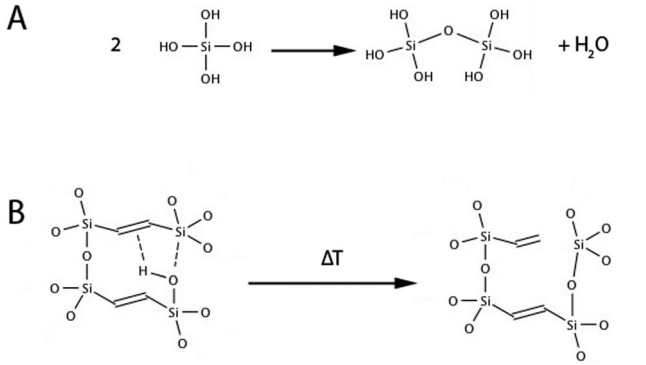

Fig. 6 The polycondensation of silicates (A) and the autohydrophobisation illustrated for ethene PMOs (B).

Remarkably the spray dried MCM-41 has a higher condensation degree than the other MCM-type materials. This higher degree of condensation cannot be correlated to the wall thickness, because this is comparable with the other MCM type materials. However, this can be explained by the synthesis procedure. During the spray drying process, sol droplets are atomized and evaporated at 220 °C.

This is a much higher condensation temperature than for the hydrothermal synthesis of MCM and SBA type materials, which typically does not exceed 110 °C. Additionally the ageing step usually applied to promote further condensation and reordering of the structure after precipitation is not present in spray dried samples. This high temperature of spray drying combined with the rapid and constant evaporation of the solvent and the ethanol produced by the hydrolysis of the ethoxy functions of the silane, will eventually result in a higher degree of condensation.

The OH species for ethene PMOs. In comparison with the chemical shifts of the silicon atoms of pure silica materials in ^{29}Si MAS NMR, a significant and distinct shift occurs for organosilica materials.[25] The spectrum and a schematic overview of the different T sites are depicted in Fig. 5. No Q sites were measured which indicates that no ethene bridges were broken during the synthesis of the silica material.

Table 4 depicts the quantified silicon species from this spectrum. Column 1 depicts the total silanol number obtained with *in situ* IR spectroscopy. Columns 2 and 3 show the T^2 : T^3 and T^1 : T^3 ratios of the ethene PMO material. Columns 4 and 5 give the respective percentages of single (T^2) and geminal (T^1) silanol groups.

Column 6 depicts the total percentage of hydroxylated silicon atoms and column 7 shows the degree of condensation. When the total amount of OH species (columns 1 and 6) is compared with these on pure silica materials (Table 3: columns 1 and 6), there are more hydroxyl groups present in the organosilica material. This is reflected in a much lower (below 50%) degree of condensation (column 7). Two different mechanisms lead to these differences. First of all the polycondensation reaction of the ethene bridged precursor molecule does not progress to completion because there are six siloxane bridges to be formed per precursor molecule instead of the four siloxane bridges to be formed for TEOS. (See the T^3 sites in Fig. 5). This is sterically more difficult than the polycondensation reaction with TEOS, used in the synthesis of MCM and SBA type materials. The second and probably the largest influence on the degree of condensation, is the temperature of the post treatment. While pure silica materials are calcined at 550 °C, organosilicas obviously are not. The surfactant that acts as the porogen inside the Periodic Mesoporous Organosilicas is typically extracted by Soxhlet extraction with acetone or ethanol.[21] The materials are never exposed to temperatures above 120 °C. When PMOs are treated at temperatures above 200 °C, the residual silanols will be further reduced by interaction with the ethene bridge, *via* an autohydrophobisation reaction, as described by Ozin *et al.*[26] and Vercaemst *et al.*[27] Finally, as the temperature reaches 300 °C, the organic bridges are destroyed.

These reactions are shown in Fig. 6.

3.4 Determination of the maximum loading of the probing molecules

The maximum loading of the materials was determined *via* the grafting procedure of three silanes that differ in carbon chain length. Through the accessible silanol groups, the probing molecules were anchored to the surface. The amount of probing molecules was quantified on the carbon amount determined with elemental analysis.

Table 5 depicts the loading capacity of the various (organo)-silica materials for a trimethylsilyl (C3), an octyldimethylsilyl (C8) and an octadecyldimethylsilyl (C18) group.

The pore diameter has been added for reference. From this table it can be observed that for the same reaction time the amount of grafted groups drops with the length of the aliphatic chain. The coverage with C18 chains is very low for all mesoporous materials. The same trend has been shown as a function of the pore size of MCM materials by Waksburg *et al.*[28]

A first interesting observation can be made when SBA-15 is compared with SBA-16 and MCM-41 with MCM-48. The cubical pore systems (SBA-16 and MCM-48) systematically have a larger amount of C18 groups anchored to the surface. This is due to the fact that a cubical pore system is accessible from three dimensions while a hexagonal pore system just from one dimension. Therefore it is clear that the inside of an SBA-16 and an MCM-48 particle can be reached more easily and thus faster than the inside of an SBA-15 and MCM-41 particle. This

Table 5 The loading capacity for relevant chromatographic groups for various ordered mesoporous (organo)silica materials

Material	Pore size nm	C3		C8		C18	
		mmol g^{-1}	groups per nm^2	mmol g^{-1}	groups per nm^2	mmol g^{-1}	groups per nm^2
SBA-15	6.9	1.8	1.7	0.7	0.7	0.1	0.1
SBA-16	6.2	2.3	1.9	0.8	0.7	0.5	0.4
MCM-41	2.9	2.2	1.2	0.9	0.5	0.4	0.2
MCM-48	2.8	2.5	1.2	1.2	0.6	0.5	0.3
MCM-41(SD)	2.9	1.9	1.6	1.0	0.8	0.3	0.3
EthenePMO	6.2	1.1	0.7	0.8	0.5	0.4	0.2
Nucleosil	~30	0.4	2.8	0.5	3.3	0.3	1.9

easy access to the whole of the pore system from multiple dimensions is the reason the carbon loading on cubic pore systems is higher than the loading on hexagonal pore systems.[29]

This theory is confirmed by Nucleosil where the amount of grafted groups per nm^2 is much higher in comparison with the other materials.

The Nucleosil material consists of perfect spheres with large disordered pores (~30 nm). This much higher loading for Nucleosil confirms that the grafting procedure for porous systems is strongly diffusion regulated. The influence of diffusion is larger for the longer and more bulky grafting molecules than for the smaller ones and is larger for the hexagonal one-dimensional pore systems than for the cubic three-dimensional pore systems.

However when the molar amount of groups per weight unit (mmol g^{-1}) is considered it is immediately clear that the ordered mesoporous materials exhibit a much higher loading than the commercial Nucleosil material.

A second observation is the higher surface silanol loading of the SBA-type materials, compared to the MCM-type materials, regardless of the mesoscopic structure. This is particulary evident for the silanols that are accessible to the smallest silanes (C3, HMDS). This fact finds its origin in the synthesis methods. The SBA-type materials are synthesized by Pluronic surfactants, which are ethyleneoxide–propyleneoxide triblock copolymers. The ethyleneoxide chains create microporous perforations in the SBA-walls. The SBA-type materials (and the PMO material that was also synthesized using the Pluronic 123 surfactant) therefore have an important fraction of micropores.[30]

Table 6 shows an overview of the micropore volume and the micropore surface area of these materials. It is clear that these micropores contribute very significantly to the total pore area and could be one of the factors contributing to the higher concentration of surface accessible silanols. Although most micropores will be too small to be accessible for large silanes and even the HMDS, micropores still create an increased silanol concentration at the surface, as the pore mouths of these micropores will contain silanol groups (hydroxyl nests), that would be accessible to the silanes.

Note that the difference between the BET surface area and the sum of the micropore and the mesopore surface area based on the *t*-plot and BJH models, respectively, lies within the typical error of analysis.

3.5 Computational considerations

To get a better view on the behavior of silane groups on the silica surface, theoretical calculations were performed to determine the geometry of a carbon chain substituent. All results were obtained with the gaussian09 software package[31] using a B3LYP functional[32] with a 3-21G Pople basis set. Since the primary focus was set on determining geometries this level of theory was chosen.

First, a random silica slab was made with approximately 5.3 hydroxyl groups per nm^2. This model is designed to represent an amorphous silica surface, thus a random cluster was built with the required silanol-density. To calculate the density the total number of hydroxyl groups was divided by the exposed surface of the cluster, hydroxyl groups at the edge are only counted as half since they are also part of neighboring clusters. The proposed approach was chosen since there are no surface models available for silicas with this high silanol loading. The edges of the slab are saturated with hydrogen atoms, which were unrestricted during the optimization. One of the hydroxyl groups was exchanged with a C8 silane group. Geometry optimizations with the described methodology show the tail is oriented to minimize the interactions with the surface. This is as expected, since the apolar tail cannot interact with the polar surface (Fig. 7). Similar calculations, where an implicit solvent model (IEFPCM[33]) was added, characterized by the dielectric constant of toluene, gave comparable results. The geometrical results show that only the $-Si(CH_3)_2-$ moiety imposes a limit on the number of possible substituents per surface area. From the result it can be seen that the $-Si(CH_3)_2-$ moiety blocks at least two extra hydroxyl groups. Since those groups can also be overlapped by another silane group from a more distant position, they are only counted as half. So it can be concluded that, on this dense cluster, at least two groups are needed to accommodate the substituent leading to a maximum possible loading of 2.65 groups per nm^2.

Table 6 Overview of the micropore volume ($V_{p_{\mu,t\text{-plot}}}$) and surface area ($SA_{\mu,t\text{-plot}}$) by *t*-plot analysis; the mesopore volume ($V_{p_{m,BJH}}$) and surface area ($SA_{m,BJH}$) by BJH analysis; the total pore volume ($V_{p,\,0.95}$) taken at P/P° = 0.95 and surface area (SA_{BET}) by BET analysis of SBA-15, SBA-16 and ethene PMO

Material	SA_{BET} ($m^2\ g^{-1}$)	$SA_{\mu,t\text{-plot}}$ ($m^2\ g^{-1}$)	$SA_{m,BJH}$ ($m^2\ g^{-1}$)	$V_{p,0.95}$ ($cm^3\ g^{-1}$)	$V_{p_{\mu,t\text{-plot}}}$ ($cm^3\ g^{-1}$)	$V_{p_{m,BJH}}$ ($cm^3\ g^{-1}$)
SBA-15	655	460	429	0.84	0.07	0.74
SBA-16	738	469	398	0.63	0.11	0.47
EthenePMO	923	649	598	0.99	0.07	0.87

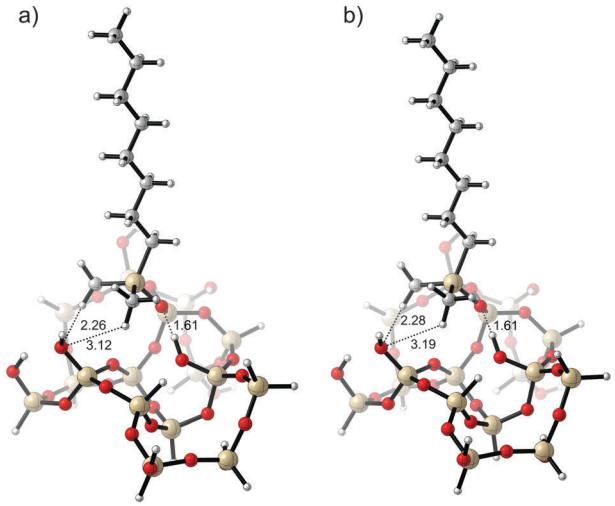

Fig. 7 Random silica surface with 5.3 hydroxyl groups per nm^2 and one C8 silane substituent. This silane blocks two neighboring silanol groups. Figure (a) is without an implicit solvent model and (b) is the same starting geometry optimized with such a model. The differences are minimal.

On a less dense surface with about 2.5 hydroxyl groups per nm^2 there are no neighboring positions blocked (Fig. 8). This means the theoretical density in this case is 2.5 groups per nm^2. On average, 2.5 groups per nm^2 is the theoretical maximal loading on a silica surface with only single silanols present, this is close to the value that can be estimated from the kinetic diameter of the silane and that was reported previously by Van Der Voort.[34]

To assess the influence of geminal silanols a slight modification on the random surface was made, an extra hydroxyl group was added on a silicon atom and one Si–O–Si bond on that atom was broken.

The other silicon atom was saturated by hydrogen. With this approach the surface contains a single geminal group. Two silane groups were placed on this site and after geometry optimization it appeared that at least two extra silanol groups were blocked by this (Fig. 9).

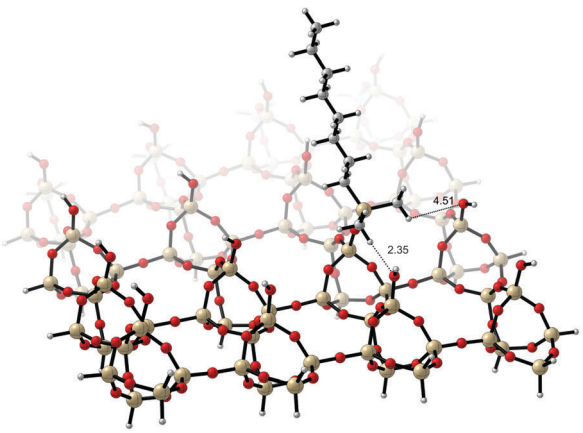

Fig. 8 Surface model with about 2.5 hydroxyl groups per nm^2 the surface is based on an ordered silica slab. The silane group is close to a neighboring hydroxyl group, but since the surface is more open this does not block the site. As an upper bound, on this type of surface it is possible to have 2.5 silane substituents per nm^2. However, when the surface is almost full, the close interaction (2.35 Å) will fully shield one of the hydroxyl groups and the theoretical maximum will never be reached.

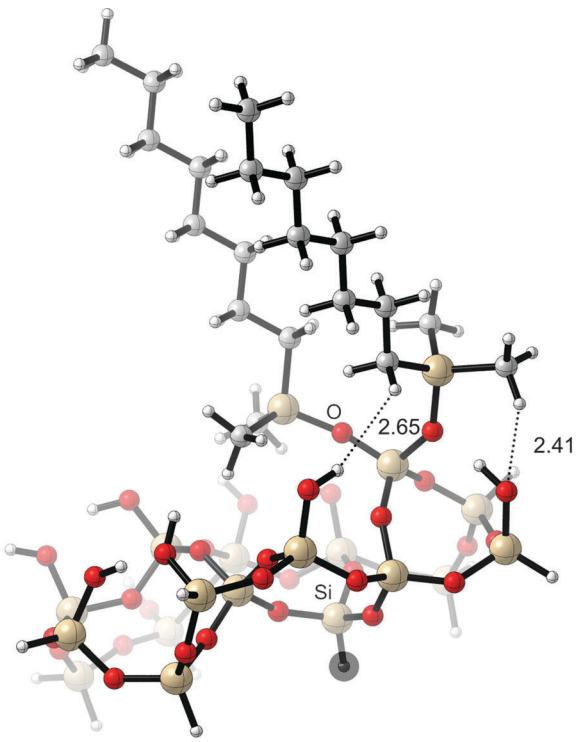

Fig. 9 The original cluster is modified to incorporate a geminal silanol, the Si–O bond between the atoms explicitly named on the figure was broken and the marked hydrogen atom was added for saturation, a second silane group was then added to the free oxygen. With two silane groups on a geminal silanol two other silanol groups are blocked. This allows a more efficient stacking of the substituents.

Table 7 The bulk silanol number, the amount of single and geminal silanols and the surface silanol groups, depicted with the pore diameter (d_p) and pore wall (h)

Material	1 $\alpha_{OH,bulk}$ (mmol g^{-1})	2 $\alpha_{OH,single,bulk}$ (mmol g^{-1})	3 $\alpha_{OH,geminal,bulk}$ (mmol g^{-1})	4 $\alpha_{OH,surface}$ (mmol g^{-1})	5 $\alpha_{OH,surface}$ (g nm^{-2})	6 h (nm)	7 d_p (nm)
SBA-15	3.5	3.1	0.4	1.8	1.7	4.2	6.9
SBA-16	8.3	8.0	0.4	2.3	1.9	6.4	6.2
MCM-41HT	3.6	3.4	0.2	2.2	1.2	1.1	2.9
MCM-48	5.2	4.9	0.2	2.5	1.2	1.0	2.8
MCM-41SD	3.2	3.1	0.1	1.9	1.6	1.2	2.9
EthenePMO	16.9	14.3	2.6	1.1	0.7	3.1	6.2

For the same reason as before they only count as half. With the extra hydroxyl group from the geminal silanol, the surface silanol density is 6.7 groups per nm^2 (the surface area remains unchanged but an extra hydroxyl group is added). This means that when one extra hydroxyl group is blocked by the silane moiety, the density of substituents on the surface can be calculated as:

$$\frac{2 \text{ silane groups } 6.7 \text{ g nm}^{-2}}{3 \text{ hydroxyl groups}} = 4.5 \text{ g nm}^{-2}$$

A fully hydroxylated silica surface (single silanol groups) can have maximum of 4.6 ± 0.5 groups per nm^2. This means that roughly only half of the single silanol groups are sterically available for grafting which coincides with previous reports on that matter.[4]

In Table 7 we summarize the total silanol number, differentiated as total, geminal and single silanols and the silanol that are accessible for the small HMDS molecule, expressed in mmol per gram and in groups per nm^2.

The amount of single and geminal silanols (columns 2 and 3 in Table 7) are calculated by multiplying the relative amount of silanols with the total number of OH groups determined by IR spectroscopy (*i.e.* $\alpha_{OH} \times (Q^3/(Q^2 + Q^3) = \alpha_{OH,single}$).

This gives the absolute amount single and geminal silanols, irrespective of their location. They could be on the pore wall or in the bulk silica.

Column 4 in Table 7 then shows the silanols that were available to the small HMDS (C3 silane). Because none of these values exceed the theoretical maximum values they can be considered as the ''surface'' or ''reachable'' silanols.

4 Conclusions

We have established that the amount of silane groups (expressed as groups per nm^2) that can be grafted on the surface of ordered mesoporous silicas (MCM-41, MCM-48, SBA-15, SBA-16) is much smaller than on the surface of the commercial materials, which are typically used as a packing material for HPLC columns. The main reason for this is that the grafting reaction is strongly diffusion limited, as the surface area of these materials is basically internal surface area.

For the mesoporous silicas, it can be concluded that the amount of surface silanols is larger for the micropore containing SBA-type materials than for the non-microporous MCM-type materials. In general, for the thick walled mesoporous silicas, one should keep in mind that up to 70% of the silanols is unreachable for a small silane.

Spray dried MCM-41 exhibits a more condensed silica structure due to the higher synthesis temperature. The PMO material (ethene PMO) on the other hand exhibits a lower condensation degree. This can be attributed to the different condensation behavior of $(EtO)_3$–Si–CH=CH–Si$(OEt)_3$ compared to Si$(OEt)_4$ and to the absence of a high temperature calcination procedure.

Acknowledgements

M.I. acknowledges the IWT-Flanders (Agentschap voor Innovatie door Wetenschap en Technologie) grant no. IWT/SB/71325 for financial support. T.B. is indebted to Ghent University, GOA-grant, project number 01G00710 and the European Research Council (FP7(2007–2013) ERC grant no. 240483). Computational resources and services were provided by Ghent University.

Notes and references

1 K. D. Bartle, R. D. Carney, A. Cavazza, M. G. Cikalo, P. Myers, M. M. Robson, S. C. P. Roulin and K. J. Sealey, *J. Chromatogr., A*, 2000, **892**, 279.
2 D. Sindorf and G. Maciel, *J. Am. Chem. Soc.*, 1983, **105**, 1487; J. Kratochvila, Z. Salajka, A. Kazda, Z. Kadlc, J. Soucek and M. Georghiu, *J. Non-Cryst. Solids*, 1990, **116**, 93; G. Kellum and R. Smith, *Anal. Chem.*, 1967, **39**, 341.
3 L. Zhuravlev, *Colloids Surf., A*, 1993, **74**, 71; L. Zhuravlev, *Langmuir*, 1987, **3**, 316; L. Zhuravlev, *Colloids Surf., A*, 2000, **173**, 1; J. Nawrocki, *J. Chromatogr., A*, 1997, **779**, 29.
4 A. Vansant, P. Van Der Voort and K. Vrancken, *Characterization and Chemical Modification of the Silica Surface; Studies in Surface Science and Catalysis*, 1995, vol. 93.
5 S. Ek, A. Root, M. Peussa and L. Hiinistö, *Thermochim. Acta*, 2001, **379**, 201.
6 B. McCool, L. Murphy and C. P. Tripp, *J. Colloid Interface Sci.*, 2006, **295**, 294; V. L. Zholobenko, D. Plant, A. J. Evans and S. M. Holmes, *Microporous Mesoporous Mater.*, 2001, **44–45**, 793.
7 S. Léonardelli, L. Facchini, C. Fretigny, P. Touyne and A. P. Legrand, *J. Am. Chem. Soc.*, 1992, **114**, 6412; C. C. Liu and G. E. Maciel, *J. Am. Chem. Soc.*, 1996, **118**, 5103.
8 C. Delitala, E. Cadoni, D. Delpiano, D. Meloni, M. D. Alba, A. I. Becerro and I. Ferino, *Microporous Mesoporous Mater.*, 2009, **118**, 11.
9 D. W. Sindorf and G. E. Maciel, *J. Am. Chem. Soc.*, 1983, **105**, 3767; D. Park, N. Nishiyama, Y. Egashina and K. Ueyama, *Ind. Eng. Chem. Res.*, 2001, **40**, 6105; H. Knözigner, P. Schuster, G. Zundel and C. Sandorfy, *Hydrogen Bond*, 1979, **3**, 1263; M. Kruk, V. Antochshuk, J. Matos, L. Mercuri and M. Jaroniec, *J. Am. Chem. Soc.*, 2002, **124**, 768.
10 E. Hansen, R. Schmidt, M. Stöcker and D. Akporiaye, *J. Phys. Chem.*, 1995, **99**, 4148; B. Grünberg, T. Emmler, E. Gedat, I. Shendrovich, G. H. Findenegg, H. Limbach and G. Buntkowsky, *Chem.–Eur. J.*, 2004, **10**, 5689; A. Lebret, G. Lelong, P. Mason, M. Saboungi and J. Brady, *Food Biophys.*, 2011, **6**, 233.
11 I. Shendrovich, A. Buntowsky, A. Schreiber, E. Gedat, S. Sharif, J. Albrecht, N. Golubev, G. Findenegg and H. Limbach, *J. Phys. Chem. B*, 2003, **107**, 11924.
12 S. Pizzanelli, S. Kababya, V. Frydman, M. Landau and S. Vega, *J. Phys. Chem. B*, 2005, **109**, 1997; H. Landmesser, H. Kosslick and R. Fricke, *Solid State Ionics*, 1997, **101–103**, 271; V. Kocherbitov and V. Alfredsson, *J. Phys. Chem. C*, 2007, **111**, 12906; A. Cauvel, F. Brunel, F. DiRenzo, E. Garrone and B. Fubini, *Langmuir*, 1997, **13**, 2773; J. Blin and C. Carteret, *J. Phys. Chem. C*, 2007, **111**, 2773; P. Sutra, F. Fajula, D. Brunel, P. Lentz, P. Daelen and J. Nagy, *Colloids Surf., A*, 1999, **158**, 21.
13 X. Zhao, G. Lu, A. Whittaker, G. Millar and H. Zhu, *J. Phys. Chem. B*, 1997, **101**, 6525; P. Llewellyn, F. Schuth, Y. Grillet, F. Rouquerol and K. Unger, *Langmuir*, 1995, **11**, 574; J. Trebosc, J. Wiench, S. Huh, U. Lin and M. Prusky, *J. Am. Chem. Soc.*, 2005, **127**, 3057; I. Shenderovitch, D. Maudu, G. Akcakayiran, G. Buntowsky, H. Limbach and G. Findenegg, *J. Phys. Chem. B*, 2007, **111**, 12088.
14 J. P. Gallas, J. M. Goupil, A. Vimont, J. C. Lavalley, B. Gil, J. P. Gilson and O. Miserque, *Langmuir*, 2009, **25**, 5825.
15 D. Y. Zhao, Q. S. Huo, J. L. Feng, B. F. Chmelka and G. D. Stucky, *J. Am. Chem. Soc.*, 1998, **120**, 6024.
16 W. J. J. Stevens, M. Mertens, S. Mullens, N. Thijs, G. Van Tendeloo, P. Cool and E. F. Vansant, *Microporous Mesoporous Mater.*, 2006, **93**, 119.
17 J. S. Beck, J. C. Vartuli, W. J. Roth, M. E. Leonowicz, C. T. Kresge, K. D. Schmitt, C. T. W. Chu, D. H. Olsen, E. W. Sheppard, S. B. Mc-Cullen, J. B. Higgins and J. L. Schlenker, *J. Am. Chem. Soc.*, 1992, **114**, 10834.

18 O. Collart, P. Van Der Voort, E. Vansant, D. Desplantier, A. Galarneau, F. Di Renzo and F. Fajula, *J. Phys. Chem. B*, 2001, **105**, 12771.
19 M. Ide, E. Wallaert, I. Van Driessche, F. Lynen, P. Sandra and P. Van Der Voort, *Microporous Mesoporous Mater.*, 2011, **142**, 282.
20 F. Goethals, C. Vercaemst, V. Cloet, S. Hoste, P. Van Der Voort and I. Van Driessche, *Microporous Mesoporous Mater.*, 2010, **131**, 68.
21 C. Vercaemst, M. Ide, B. Allaert, N. Ledoux, F. Verpoort and P. Van Der Voort, *Chem. Commun.*, 2007, 2261.
22 M. Kruk, M. Jaroniec and A. Sayari, *Chem. Mater.*, 1999, **11**, 492.
23 P. Ravikovitch and A. Neimark, *Langmuir*, 2000, **16**, 2419.
24 P. Ravikovitch and A. Neimark, *Langmuir*, 2001, **18**, 911.
25 C. Vercaemst, M. Ide, P. Wiper, J. Jones, Y. Khimyak, F. Verpoort and P. Van Der Voort, *Chem. Mater.*, 2009, **21**, 5792.
26 T. Asefa, M. MacLachlan, H. Grondey, N. Coombs and G. Ozin, *Angew. Chem., Int. Ed.*, 2000, **39**, 1808.
27 P. Van Der Voort, C. Vercaemst, D. Schaubroeck and F. Verpoort, *Phys. Chem. Chem. Phys.*, 2008, **10**, 5349.
28 A. Waksburg, M.-H. T. Nguyen, A. L. Chaffee, M. K. Kidder, A. C. Buchanan and P. F. Britt, *Mol. Simul.*, 2011, **37**, 1266.
29 M. Anderson, *Zeolites*, 1997, **19**, 220.
30 M. Kruk, M. Jaroniec, C. Hyun and R. Ryoo, *Chem. Mater.*, 2000, **12**, 1961.
31 M. J. Frisch, G. W. Trucks, H. B. Schlegel, G. E. Scuseria, M. A. Robb, J. R. Cheeseman, G. Scalmani, V. Barone, B. Mennucci, G. A. Petersson, H. Nakatsuji, M. Caricato, X. Li, H. P. Hratchian, A. F. Izmaylov, J. Bloino, G. Zheng, J. L. Sonnenberg, M. Hada, M. Ehara, K. Toyota, R. Fukuda, J. Hasegawa, M. Ishida, T. Nakajima, Y. Honda, O. Kitao, H. Nakai, T. Vreven, J. A. Montgomery Jr., J. E. Peralta, F. Ogliaro, M. Bearpark, J. J. Heyd, E. Brothers, K. N. Kudin, V. N. Staroverov, R. Kobayashi, J. Normand, K. Raghavachari, A. Rendell, J. C. Burant, S. S. Iyengar, J. Tomasi, M. Cossi, N. Rega, J. M. Millam, M. Klene, J. E. Knox, J. B. Cross, V. Bakken, C. Adamo, J. Jaramillo, R. Gomperts, R. E. Stratmann, O. Yazyev, A. J. Austin, R. Cammi, C. Pomelli, J. W. Ochterski, R. L. Martin, K. Morokuma, V. G. Zakrzewski, G. A. Voth, P. Salvador, J. J. Dannenberg, S. Dapprich, A. D. Daniels, O. Farkas, J. B. Foresman, J. V. Ortiz, J. Cioslowski and D. J. Fox, *Revision A.02*, Gaussian, Inc., Wallingford CT, 2009.
32 A. D. Becke, *J. Chem. Phys.*, 1993, **98**, 5648; C. T. Lee, W. T. Yang and R. G. Parr, *Phys. Rev. B: Condens. Matter Mater. Phys.*, 1988, **37**, 785.
33 E. Cances, B. Mennucci and J. Tomasi, *J. Chem. Phys.*, 1997, **107**, 3032.
34 P. Van Der Voort, S. Vercauteren, K. Peeters and E. Vansant, *J. Colloid Interface Sci.*, 1993, **157**, 518.

